Frequency dependence of asymmetry-induced transport in a non-neutral plasma trap

D. L. Eggleston[a] and B. Carrillo
Physics Department, Occidental College, Los Angeles, California 90041

(Received 4 November 2002; accepted 22 January 2003)

A key prediction of the theory of asymmetry-induced transport is that the particle flux will be dominated by particles that move in resonance with the asymmetry. For the case of a time-varying asymmetry, the resonance condition is $\omega - l\omega_R - n\pi v/L = 0$, where v is the axial velocity, L is the plasma length, ω_R is the $E\times B$ rotation frequency, and ω, l, and n are the asymmetry frequency, azimuthal wavenumber, and axial wavenumber, respectively. Data are presented from experiments on a low density trap in which ω, ω_R, and n are varied and the resulting radial particle flux is measured. The experiments show a resonance in the flux similar to that predicted by theory. The peak frequency of this resonance increases with ω_R and varies with n, in qualitative agreement with theory, but quantitative comparisons between experiment and theory show serious discrepancies.
 [DOI: 10.1063/1.1561276]

I. INTRODUCTION

Non-neutral plasma traps of the Malmberg–Penning type have been found to be useful in a variety of fields including basic plasma physics, atomic spectroscopy, antimatter physics, and mass spectroscopy. These traps are cylindrical in geometry and employ an axial magnetic field for radial confinement and biased end cylinders for axial confinement. Early studies of the confinement time of such traps found good agreement between experiments[1] and a transport theory[2] based on collisions with neutrals. At the lowest neutral pressures, however, the confinement time was much lower than expected[3] and decreased with machine length.[4] It was suggested that this anomalous transport was due to the presence of electric or magnetic fields that break the cylindrical symmetry of the trap. The presence of such asymmetries would produce a radial component to the $E\times B$ or grad-B drift that would lead to particle loss. This notion was later supported by further confinement studies[5] as well as experiments with applied electric[6–11] and magnetic[12–14] asymmetries.

These early papers also suggested that the asymmetry-induced transport might be described by a theoretical model developed for studies of radial transport in the early tandem mirrors[15–19] where static, asymmetric end cells produced radial grad-B drifts that largely determined the radial particle flux. A key prediction of the theory is that the resulting transport will be dominated by particles whose axial bounce motion and azimuthal drift motion causes them to move in resonance with the asymmetry. As these resonant particles repeatedly encounter the asymmetry they take radial steps in the same direction, thus allowing them to diffuse more quickly than nonresonant particles.

In this article we present experiments that test this key prediction of the theory. We do this by applying a variable frequency electrostatic asymmetry to a Malmberg–Penning trap and measuring the resulting radial particle transport as a function of the asymmetry frequency. Our modified trap design avoids previously encountered complications produced by collective effects and allows for a clean test of the transport physics. While the experimental results are qualitatively consistent with theory and seem to confirm the dominant role played by resonant particles, the frequency dependence of the transport does not quantitatively match the predictions of theory.

II. ASYMMETRY-INDUCED TRANSPORT THEORY AND EXPERIMENTAL APPROACH

Our experiments are performed in a modified Malmberg–Penning trap in which the plasma has been replaced by a biased wire and the transport of low density test particles is studied. This experimental approach is best understood in the context of asymmetry-induced transport theory, so we begin with a summary of the theory as recently adapted to Malmberg–Penning traps and allowing for electric field asymmetries at a nonzero angular frequency ω.[20] The theory assumes a cylindrical geometry with an axial magnetic field B_z. In typical experiments, the magnetic field is strong enough that the Larmor radius is much smaller than any other scale length in the plasma and all relevant frequencies are small compared to the cyclotron frequency. Asymmetric electric fields are applied by placing voltages on wall sectors. Under these conditions, the basic equations for a non-neutral plasma are Poisson's equation, the drift kinetic equation with a collision operator, and the boundary conditions on the conducting walls. For simplicity, a plasma of length L with flat ends is assumed and end effects are ignored. This allows for the linearization of the potential as $\phi(r,\theta,z,t) = \phi_0(r) + \phi_1(r,\theta,z,t)$, where

$$\phi_1(r,\theta,z,t) = \sum_{n,l,\omega} \phi_{nl\omega}(r)\cdot\exp\left[i\left(\frac{n\pi}{L}z + l\theta - \omega t\right)\right] \quad (1)$$

[a]Electronic mail: eggleston@oxy.edu

is the asymmetry potential. A similar linearization is employed for the distribution function f. For an electron plasma ($q=-e$), Poisson's equation then becomes

$$\left[\frac{1}{r}\frac{d}{dr}r\frac{d}{dr}-\frac{l^2}{r^2}-\left(\frac{n\pi}{L}\right)^2\right]\phi_{nl\omega}(r)$$

$$=4\pi e\int dv\frac{(cl/rB_z)(\partial f_0/\partial r)-(n\pi/L)(e/m)(\partial f_0/\partial v)}{(n\pi/L)v+l\omega_R-\omega-i\nu_{\text{eff}}}$$

$$\times\phi_{nl\omega}(r), \tag{2}$$

where ω_R is the azimuthal $E\times B$ rotation frequency of the plasma column, $\phi_{nl\omega}(r)$ is the Fourier amplitude of the asymmetry mode characterized by axial mode number n, azimuthal mode number l, and angular frequency ω, ν_{eff} is the effective collision frequency, f_0 is the unperturbed distribution function (assumed Maxwellian), and the integral is over the axial velocity v.

The form of the resulting radial particle flux depends on the relative size of the effective collision frequency ν_{eff} and the oscillation frequency ω_T of particles trapped in the asymmetry potential, where $\nu_{\text{eff}}^3\approx\nu_{ee}(n\pi\bar{v}/L)^2$ and

$$\omega_T^2=\left[\frac{e}{m}\left(\frac{n\pi}{L}\right)^2-\frac{cl^2}{rB_z}\frac{d\omega_R}{dr}\right]\phi_{nlw}(r). \tag{3}$$

When $\nu_{\text{eff}}\gg\omega_T$, frequent collisions interrupt the trapped particle orbits and the basic radial step is the radial drift velocity multiplied by the time between collisions. Deviations from unperturbed orbits are small and a perturbation approach is appropriate. This is called the resonant plateau regime. When $\nu_{\text{eff}}<\omega_T$, a trapped particle can complete at least one oscillation before a collision knocks it out of resonance. Now the basic radial step is the radial extent of the drift during a trapping oscillation and the orbits are fully nonlinear. A heuristic derivation of the resulting radial flux is often employed for this "banana" regime. The resulting radial particle flux for the plateau regime is given by (see Ref. 20 for details)

$$\Gamma_{\text{plateau}}=-\sum_{n,l,\omega}\frac{n_0}{\sqrt{2\pi\bar{v}^2}}\frac{L}{|n|}\left|\frac{cl\phi_{nl\omega}(r)}{rB_z}\right|^2$$

$$\times\left[\frac{1}{n_0}\frac{dn_0}{dr}+\sqrt{2}\frac{n\pi}{L}\frac{r\omega_c}{l\bar{v}}x\right]e^{-x^2} \tag{4}$$

and for the banana regime by

$$\Gamma_{\text{banana}}$$

$$=-\sum_{n,l,\omega}\frac{n_0}{\sqrt{2\pi}}\frac{\nu_{ee}(L/n\pi)^2(l\bar{v}/r\omega_c)^2(e\phi_{nl\omega}(r)/T)^{1/2}}{\{1-(lL/n\pi)^2(1/r\omega_c)(d\omega_R/dr)\}^{3/2}}$$

$$\times\left[\frac{1}{n_0}\frac{dn_0}{dr}+\sqrt{2}\frac{n\pi}{L}\frac{r\omega_c}{l\bar{v}}x\right]e^{-x^2}. \tag{5}$$

For simplicity, we have assumed here that the temperature T is constant with radius. The variable x is equal to $v_{\text{res}}/\sqrt{2}\bar{v}$, where

$$v_{\text{res}}=\frac{L}{n\pi}(\omega-l\omega_R) \tag{6}$$

is the resonant velocity for the asymmetry mode n,l,ω. The symbols n_0, $\bar{v}$, ω_c, and ν_{ee} denote the electron density, thermal velocity, cyclotron frequency, and the electron-electron collision frequency, respectively.

It is worth noting several features of these solutions. Both plateau and banana regime fluxes involve a sum over all the asymmetry modes produced by the wall voltages. The square brackets (which are common to both regimes) contain a diffusive term $(1/n_0)(dn_0/dr)$ and a generalized mobility $\sqrt{2}(n\pi/L)(r\omega_c/l\bar{v})x$ (note that this latter term reduces to eE/kT for $\omega=0$). The plateau regime flux is independent of the collision frequency and is proportional to the square of the asymmetry amplitude $\phi_{nl\omega}^2$, whereas the banana regime flux depends linearly on ν_{ee} and scales like $\phi_{nl\omega}^{1/2}$. Our previous studies of the amplitude scaling[11] suggest that we are in the plateau regime, but the results of this article are not dependent upon that identification because both regimes have the same frequency dependence. The previously mentioned domination of the transport by resonant particles is reflected in the e^{-x^2} factor, which stems from evaluating the Maxwellian distribution function at the resonant velocity. Note that x can be positive or negative since ω may be greater than or less than ω_R. Here, we use the convention that $\omega>0$ corresponds to an asymmetry that rotates with the plasma column and $\omega<0$ corresponds to one that rotates against the column. When the second term in the square brackets dominates over the first, a static field asymmetry ($\omega=0$, $x<0$) will move electrons radially outward ($\Gamma>0$), but an appropriately chosen asymmetry ($\omega>\omega_R$, $x>0$) can move particles radially inward. Such inward transport has been observed in "rotating wall" experiments.[6,8,21–23]

The presence of ω in the variable x provides the experimentalist with an ideal way of testing the notion that resonant particles dominate the transport. By varying ω, one can obtain any value of the resonant velocity v_{res} [see Eq. (6)] while keeping other experimental parameters fixed. The resulting radial flux should then exhibit a resonance as v_{res} sweeps through the distribution function. The ability to place v_{res} in the bulk of the distribution function also makes it possible to obtain a measurable amount of radial transport while keeping the asymmetry amplitude low. This approach, however, is complicated by the strong ω-dependence of the asymmetry potential $\phi_{nl\omega}(r)$ in the plasma. Numerical solutions of Eq. (2) for typical plasma parameters[20] show that the transport-producing electric field in the plasma (i.e., $E_\theta=l\phi_{nl\omega}/r$) can vary by many orders of magnitude as adjustments of ω produce plasma phenomena ranging from standing waves to Debye shielding. These variations in E_θ (and thus in the radial flux Γ) tend to dominate or mask those produced by resonant particle effects. This produces, for example, enhanced transport when the asymmetry drives a helical standing wave of the plasma column as was observed in previous experiments.[6,21–23] It is also possible for the applied asymmetries to drive nonlinear collective processes,[24] and such behavior has been observed experimentally.[25] While these collective processes are interesting, they are not essential to the transport physics. In this context we note that the numerical solutions of Eq. (2) also show that the variations

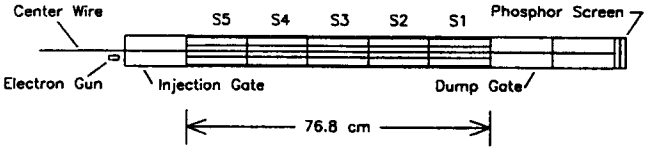

FIG. 1. Schematic of the Occidental College Trap. The usual plasma column is replaced by a biased wire to produce the basic dynamical motions in low density electrons injected from an off-axis gun. The low density and high temperature of the injected electrons largely eliminate collective modifications of the vacuum asymmetry potential. The five cylinders (labeled S1–S5) are divided azimuthally into eight sectors each. These 40 wall sectors allow the application of single Fourier-mode asymmetries.

of E_θ with ω can be reduced as the temperature is increased or the density is reduced.

These considerations led us to employ the modified trap design shown in Fig. 1. The axial magnetic field and negatively biased end cylinders of the standard trap design are retained, but the plasma is replaced by a thin biased wire (0.356 mm diameter) suspended along the axis of the trap. This wire provides a radial electric field to replace the field normally produced by the plasma column and allows low density electrons injected into this device to have the same zeroth-order dynamical motions as those in a typical nonneutral plasma (axial bounce and azimuthal $E\times B$ drift motions). The collective variations of $\phi_{nl\omega}(r)$, however, are minimized since the lower density (10^5 cm^{-3}) and higher temperature (4 eV) of the electrons give a Debye length ($\lambda_D=4.7$ cm) larger than the trap radius ($R=3.82$ cm). Under these conditions, the applied asymmetry potentials are essentially the vacuum potentials (their ω-dependence is eliminated). In short, we have constructed a trap where the electrons will act as test particles moving in the prescribed fields. Despite these changes, the confinement time scaling with no applied asymmetries[26] shows the same $(L/B)^2$ dependence found in higher density experiments,[4,5] supporting the notion that the radial transport is primarily a single particle effect.

Experiments studying asymmetry-induced transport typically use azimuthally sectored cylinders in the confinement region to apply asymmetric electric fields. In our device, we have sectored the entire confinement region (five cylinders, labeled S1–S5 in Fig. 1, with eight azimuthal divisions each) for two reasons. The first reason is to ensure that the applied potentials stay small enough for the theory to be valid. When the potential ϕ_W is applied on a single sector of length L_s, the amplitude of the Fourier modes will be proportional to $(L_s/L)\phi_W$, where L is the length of the plasma. The smaller L_s/L is, the larger the wall potential necessary to produce a mode $\phi_{nl\omega}$ of given amplitude and thus a given amount of transport. The amplitude of the wall potential, however, is not unrestricted: linear theory assumes the trajectories of the electrons are not radically different from the unperturbed case, and thus requires $e\phi_W \ll kT_e$. In order to satisfy the theoretical assumptions while producing an observable amount of transport, it is thus advantageous to sector the entire confinement region.

The second reason for our modifications to the confinement region is to allow a clean, unambiguous test of theory. As previously noted, the theoretical expressions for the radial flux involve a sum over Fourier modes with each mode contributing to the total transport. Experimental measurement of the flux, however, produces a single number Γ. Comparison to a theoretical expression that involves a sum over terms will therefore always be somewhat ambiguous since the combination of terms producing a given flux value is not unique. The least ambiguous case would involve a single Fourier mode, but this requires many wall sectors. Forty sectors is a number that can be reasonably handled and represents a great improvement over previous experiments. By judiciously selecting the amplitude and phase of the signals applied to each sector, we can produce an asymmetry that is essentially a single Fourier mode, with higher harmonics typically having amplitudes smaller than 10% of this mode's. For these experiments, we used a helical standing wave of the form

$$\phi(r,\theta,z,t)=\phi_W\frac{r}{R}\cos\left(\frac{n\pi z}{L}\right)\cos(l\theta-\omega t), \tag{7}$$

where ϕ_W is the asymmetry potential at the wall (typically 0.2 V), R is the wall radius (3.82 cm), L is the length of the confinement region (76.8 cm), and z is measured from one end of the confinement region. This asymmetry, which decomposes into oppositely propagating helical modes, will allow particles to maintain resonance with the asymmetry when they bounce off the ends of the trap and change direction. For most of this work, the wall sectors are configured to give an asymmetry where the $n=1$, $l=1$ mode is dominant. By adjusting the relative phase of the applied signals, the asymmetry can be made to rotate either with the zeroth-order azimuthal drift ($\omega>0$) or against it ($\omega<0$).

With the frequency dependence of $\phi_{nl\omega}(r)$ eliminated by increasing the Debye length and the sum over modes removed by the strategic use of multiple wall sectors, the expression for the flux can be simplified to

$$\Gamma=-C[A+Bx]e^{-x^2}, \tag{8}$$

where $A=dn_0/dr$, $B=\sqrt{2}n_0 r\omega_c n\pi/(l\bar{v}L)$, and C contains the remaining factors in either Eq. (4) or (5). The remaining frequency dependence is contained in the normalized resonance velocity x. As the asymmetry frequency is varied, the flux will have extrema when $d\Gamma/dx=0$. Applying this to Eq. (8) and solving for x gives

$$x_{\text{peak}}=\frac{1}{2}\left[-\frac{A}{B}\pm\sqrt{\left(\frac{A}{B}\right)^2+2}\right] \tag{9}$$

or

$$\omega_{\text{peak}}=l\omega_R+\frac{\sqrt{2}}{2}\frac{n\pi}{L}\bar{v}\left[-\frac{A}{B}\pm\sqrt{\left(\frac{A}{B}\right)^2+2}\right]. \tag{10}$$

Note that the solutions for x_{peak} depend only on the ratio A/B. The two solutions correspond to two flux peaks of opposite signs, with the plus sign corresponding to flux minima and the minus sign corresponding to flux maxima. Because of the Gaussian dependence on x in Eq. (8), often only one of these peaks will be sizable.

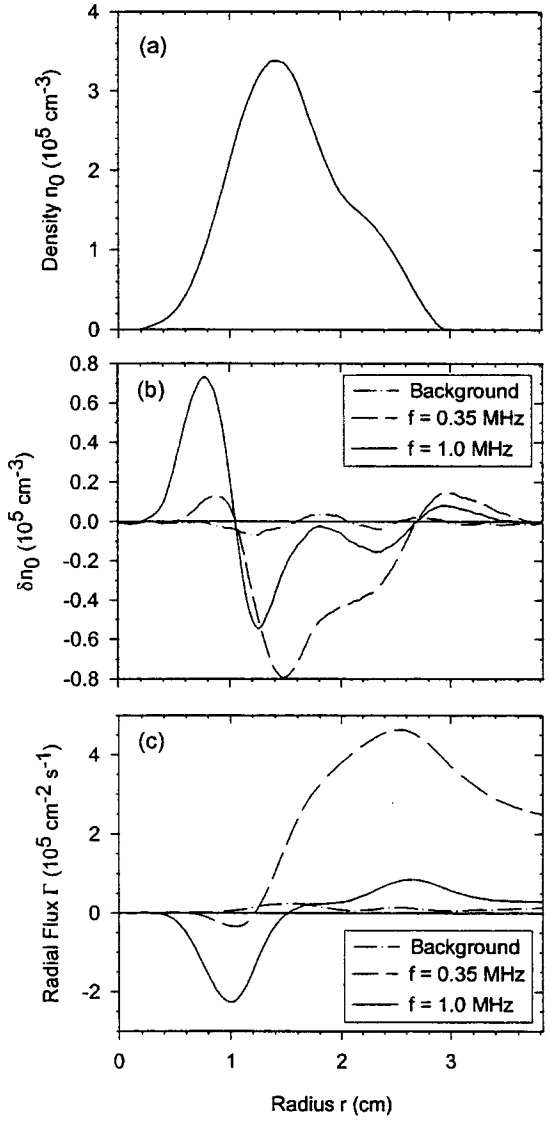

FIG. 2. Sample data showing (a) a typical density profile n_0, (b) the change in density due to asymmetries δn_0, and (c) the calculated radial flux Γ versus radial position r. Results for two typical asymmetry frequencies are shown to emphasize the frequency dependence of the transport. The relatively small background transport is also shown.

The remaining features of the trap have been discussed in detail elsewhere.[26,27] Electrons injected into the trap from an off-axis gun are quickly dispersed into an annular distribution. At a chosen time (here, 1600 ms after injection), the asymmetries are switched on for a period of time δt (here, 100 ms) and then switched off. For our experimental parameters, $\nu_{\text{eff}} \approx 50$ kHz and $\nu_{\text{eff}} \delta t \approx 5000$. At the end of the experiment cycle, the electrons are dumped axially onto a phosphor screen and the resulting image is digitized using a 512×512 pixel charge-coupled device camera. A radial cut through this image gives the density profile $n_0(r)$ of the electrons as shown in Fig. 2(a). Calibration is provided by a measurement of the total charge being dumped. Profiles are taken both with the asymmetry on and off, and the resulting change in density $\delta n_0(r)$ is obtained. Representative data for two typical asymmetry frequencies are shown in Fig. 2(b). Also shown is the background transport which is typically

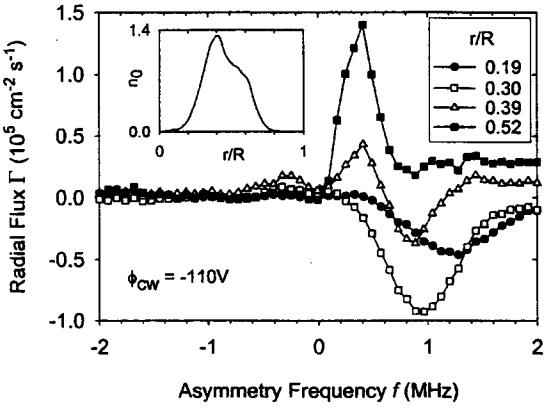

FIG. 3. Radial particle flux at four selected radii as a function of asymmetry frequency for center wire bias $\phi_{cw} = -110$ V, magnetic field $B_z = 364$ G, and Fourier mode numbers $n = 1$, $l = 1$. The shape of the flux curves is qualitatively consistent with that expected from theory. Positive frequencies correspond to experiments where the asymmetry is rotating in the direction of the electron's azimuthal $E \times B$ drift and negative frequencies correspond to counter-drift rotations. The electron density n_0 (10^5 cm^{-3}) versus scaled radius r/R is shown in the inset.

small compared to the induced transport. If the asymmetry amplitude is small enough and the asymmetry pulse length δt short enough, then $\delta n_0(r)$ will increase linearly in time. We may then approximate $dn_0/dt \simeq \delta n_0(r)/\delta t$ and calculate the radial particle flux $\Gamma(r)$ [assuming $\Gamma(r=a)=0$]:

$$\Gamma(r) = -\frac{1}{r}\int_a^r r' dr' \cdot \frac{dn_0}{dt}(r'). \tag{11}$$

Here a is the radius of the central wire. The resulting flux data are shown in Fig. 2(c). The entire experiment is then repeated for a series of asymmetry frequencies and the resulting flux versus radius and frequency data saved for analysis.

III. EXPERIMENTAL RESULTS

A typical result is shown in Fig. 3 where we plot the radial flux Γ vs asymmetry frequency f for four selected radii. The radial density profile is shown in the inset. In this plot, we follow the convention of using positive frequencies to represent experiments where the asymmetry is rotating in the direction of the electron's azimuthal $E \times B$ drift and negative frequencies to represent counter-drift rotations. There are several things to note in this figure. First, note that the predominant flux peaks occur only for positive frequencies. This is in marked contrast to other experiments[6,21–23] where driven plasma modes (which occur for both positive and negative frequencies) dominated the transport and produced flux peaks for both positive and negative frequencies. The data thus support the conclusion that we have effectively limited the role of collective modes in the experiment. Second, the fact that the flux peaks occur only for positive frequencies is in qualitative agreement with theoretical expectations. As Eq. (8) shows, the frequency dependence of the theoretical flux is constrained by the factor e^{-x^2}, a Gaussian curve centered where $\omega = \omega_R$. Since ω_R is a positive quantity and the Gaussian width $\Delta f = \sqrt{2} n \bar{v}/L$ here is about 1.5

MHz, the flux produced by negative frequencies is expected to be small. Finally, note that both positive and negative fluxes are observed and that the flux peaks occur at different frequencies. This also seems to be qualitatively consistent with the theory. When the density gradient is large, the first term in the square brackets of Eq. (8) will dominate and we expect a bell-shaped curve, opposite in sign to dn_0/dr, centered around $\omega=\omega_R$. This behavior is shown by the curves for r/R equal to 0.19, 0.30, and 0.52. Note that in our experiment ω_R is set by the center wire bias ϕ_{cw} and decreases with radius

$$\omega_R=\frac{-c\phi_{cw}}{r^2B_z\ln(R/a)}, \tag{12}$$

and thus it is expected that the flux resonances will shift to lower frequencies with radius, as observed. Near the top of the density profile, the gradient is near zero, so the second term in the square brackets of Eq. (8) will dominate. We then expect an xe^{-x^2} behavior, consistent with the shape of the $r/R=0.39$ curve.

To further check that the resonances are associated with ω_R, we have varied the center wire bias ϕ_{cw}. The results are shown in Fig. 4 (now plotting only the positive frequencies). As expected, the flux resonances maintain their general shapes but shift to higher frequencies as the magnitude of ϕ_{cw} is increased.

It is of interest to note that the distinctive experimental signatures shown in Figs. 3 and 4 depend on the full use of our wall sectors. Although we have not conducted an extensive study of this effect, it is clear that the distinctive features we have noted are washed out if too few sectors are used to apply the asymmetry. This loss of features is seen if we drive only the eight sectors of S1, the 16 sectors of S1 and S5, or the 16 sectors of S2 and S4. This is significant because the first two of these configurations are commonly used in experiments with applied asymmetries. The features are also seriously altered but still recognizable when we drive the 16 sectors of S1 and S2 only.

We have also verified that the resonances shift to lower frequencies as the axial magnetic field B_z is increased. These data are shown in Fig. 5 using an alternate method of displaying the frequency dependence of the flux: we plot the frequency at which the flux has an extremum, f_{peak}, versus radius for four different values of the magnetic field B_z. Data corresponding to both positive and negative flux peaks are shown. The trends are clear: the value of f_{peak} decreases with both magnetic field and radius. Again, this is as expected since we anticipate that f_{peak} depends on the rotation frequency $f_R=\omega_R/2\pi$. The stair-step character of the data is mainly a reflection of the limited number of frequencies (typically 26) in our data set, but noise also becomes a factor as the magnitude of the flux peak decreases.

As seen in Eq. (10), the theory also predicts a variation of f_{peak} with axial mode number n. To check this, we applied $n=2$ and 3 asymmetries to the wall sectors. The results are shown in Fig. 6 along with data from the $n=1$ configuration. The upward shift of f_{peak} with n is clear, and the inset of the figure shows that f_{peak} increases linearly with n for three

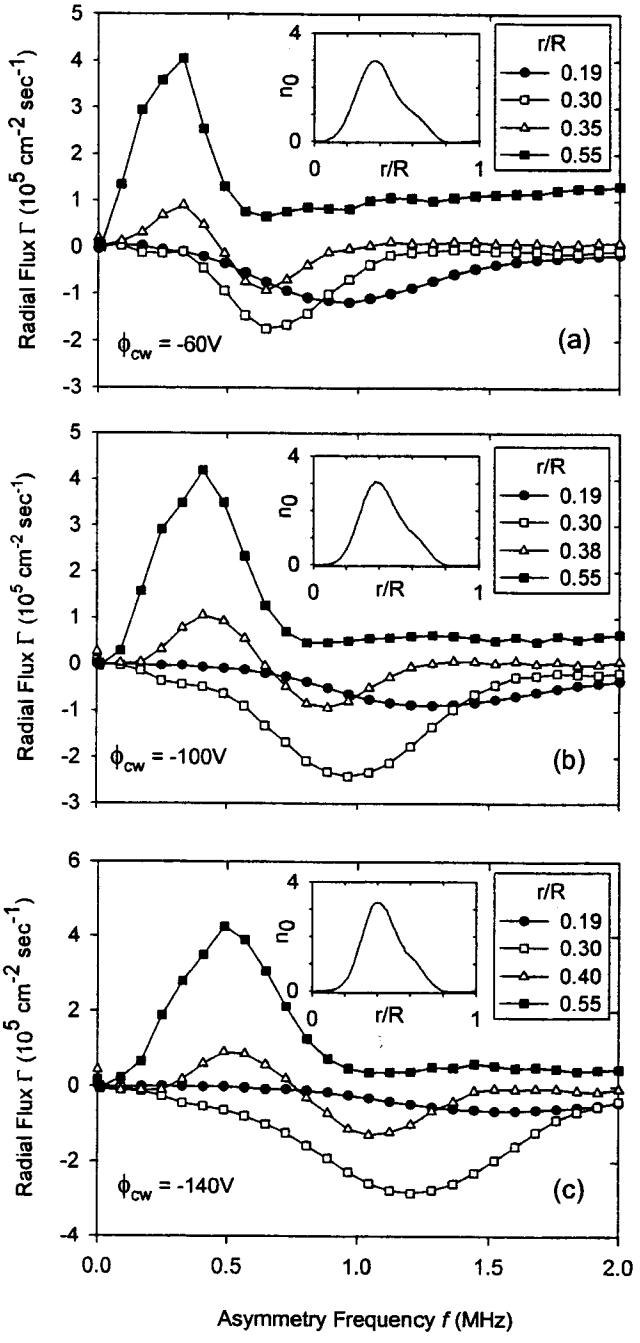

FIG. 4. As the center wire bias is made more negative, the shape of the flux resonances remains generally the same but the resonances shift to higher frequencies. This is qualitatively consistent with theory. Here, $B_z=364$ G and the center wire bias ϕ_{cw} values are (a) -60 V, (b) -100 V, and (c) -140 V. The electron density n_0 (10^5 cm^{-3}) versus scaled radius r/R is shown in the inset.

representative radii. The n-dependence of Eq. (10) is not simple (note that $B\propto n$), but deviates only slightly from linearity for experimental values of A/B and n ($-1<nA/B<2$). The observed n-dependence is thus consistent with Eq. (10) for the flux minima data. For the flux maxima data, however, Eq. (10) predicts that f_{peak} will decrease with n, in contrast to the observed increase with n. Nevertheless, the dependence of f_{peak} on n shows that the transport we are studying depends on axial variation in the asymmetry, in contrast to earlier work on radial transport induced by n

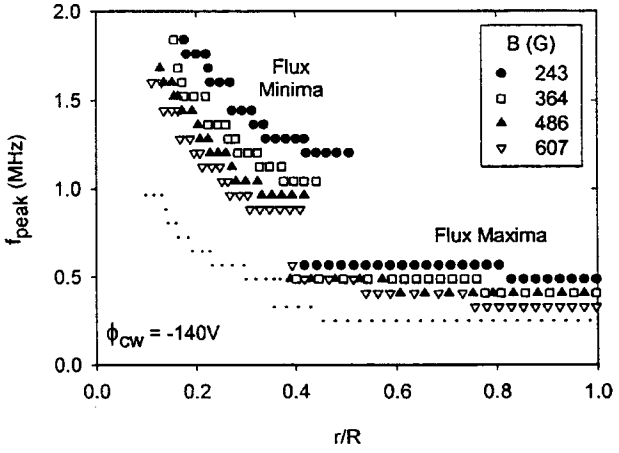

FIG. 5. As an alternate way of displaying the frequency dependence of the transport, we plot the frequency at which the flux has an extremum, f_{peak}, versus radius for four different values of the magnetic field B_z (243, 364, 486, and 607 G). The points in the upper left portion of the graph give the frequencies at which the flux is a minimum while the points in the lower right portion of the graph correspond to frequencies of flux maxima. As expected, f_{peak} decreases with both r and B_z. Here, ϕ_{cw} is -140 V. To show the range of variation, the dotted line gives data for $B_z=607$ G and $\phi_{cw}=-60$ V. For clarity, only a fraction of the 250 radial points measured are plotted.

$=0$ diocotron waves.[28] We have also verified that f_{peak} shifts upward appropriately for $l=2$.

The dependence of f_{peak} on ϕ_{cw}, B_z, and r obeys an empirical scaling law, as shown in Fig. 7. Data with ϕ_{cw} values from -20 to -140 V and B_z values from 243 to 607 G were scaled according to $f_{scaled}=f_{peak}\sqrt{B_z/-\phi_{cw}}$ and plotted versus r/R. The number of radial points plotted for each case was reduced for clarity. Although there is some scatter in the data, a fairly good universal curve is formed. The frequencies for the flux minima also scale inversely with the square root of the radius, as shown by the solid line. The scaling law for these points is thus

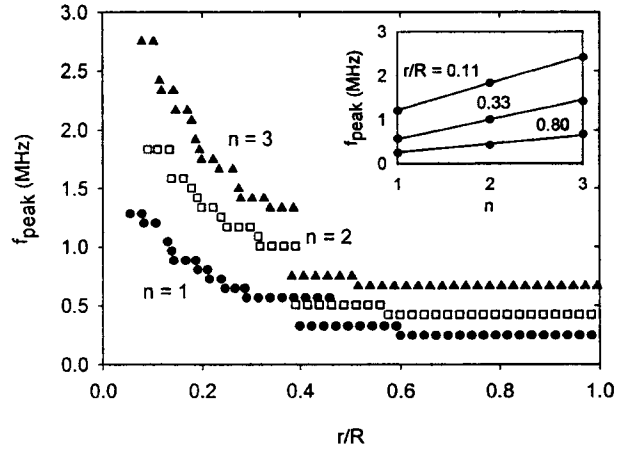

FIG. 6. f_{peak} vs r for three values of the axial mode number n. Again, the points in the upper left portion of the graph give the frequencies at which the flux is a minimum while the points in the lower right portion of the graph correspond to frequencies of the flux maxima. A linear increase of f_{peak} with n is shown in the inset for three representative values of scaled radius r/R. Here, $\phi_{cw}=-146$ V and $B_z=364$ G.

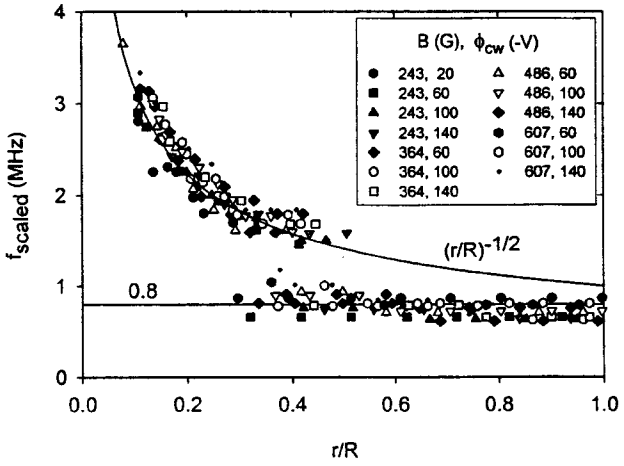

FIG. 7. Empirical scaling of f_{peak}. Data having various values of B_z and ϕ_{cw} were scaled according to $f_{scaled}=f_{peak}\sqrt{B_z/-\phi_{cw}}$ and plotted versus the scaled radius r/R. Solid lines show simple "universal" curve fits to the resulting data points.

$$f_{peak}(\mathrm{MHz})=\sqrt{\frac{-\phi_{cw}(\mathrm{V})}{B_z(\mathrm{G})}}\frac{R}{r}.$$

The frequencies for the flux maxima decrease slightly with radius, but the scatter in the data is too large to validate a particular radial dependence. If we ignore the radial variation, we obtain the rough scaling law

$$f_{peak}(\mathrm{MHz})=0.8\sqrt{\frac{-\phi_{cw}(\mathrm{V})}{B_z(\mathrm{G})}}.$$

As we have shown, the parametric dependence of f_{peak} on ϕ_{cw}, B_z, r, and, for the flux minima, n is qualitatively consistent with theory (i.e., f_{peak} increases and decreases appropriately). A quantitative comparison of experiment and theory, however, reveals serious discrepancies. To illustrate this, we have used experimental values to evaluate Eq. (10) and found f_{peak} as a function of radius r for the case where $n=1$, $l=1$, $B_z=364$ G and $\phi_{cw}=-146$ V. The results are shown in Fig. 8 along with the experimental data and the calculated f_R. While the experimental frequencies for the flux minima (solid circles) match the theory for $r/R\simeq 0.4$, they clearly diverge from theory at smaller radii. More seriously, the theory for these negative flux peaks constrains f_{peak} to be greater than the rotation frequency f_R, but the experimental data clearly cross the f_R line, shown dotted in the figure. Flux minima data for $n=2$ and 3 show similar behavior and a similar level of agreement. The data for the frequencies of the flux maxima (open circles) do not match the theory at any point. The theory for the positive flux peak shows f_{peak} going smoothly through zero to include negative values, while the experimental values always remain positive. Indeed, the experimental Γ vs f curves (cf. Figs. 3 and 4) seem to indicate that asymmetry frequencies near zero are anomalously ineffective at producing transport. Finally, as noted above, the theory has f_{peak} for the flux maxima decreasing with n, whereas the experiment shows an increase with n.

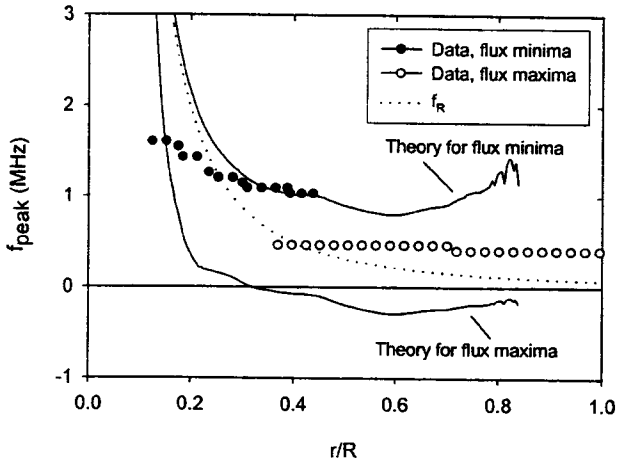

FIG. 8. Comparison of experimental and theoretical values for f_{peak}. Experimental density profiles are used in Eq. (10) to produce the theory curves shown by the solid lines. Experimental data are also shown for this case, where $B_z = 364$ G and $\phi_{cw} = -146$ V. The rotation frequency f_R is represented by the dotted line for comparison.

IV. DISCUSSION

There are several simplifying assumptions made in the theory which may account for the discrepancies between theory and experiment. The theory used here assumes that the plasma particles specularly reflect at the ends of the trap and that this reflection point is the same at all radii (i.e., L is not a function of radius). The theory also assumes that the rotation frequency ω_R is not a function of axial position z. While these assumptions are clearly violated in our experiment, our preliminary studies of these effects give corrections to the theory that are too small to account for the observed discrepancies.

The theory used here also assumes that the plasma temperature T is constant with radius. A radial temperature variation would add a term $(n_0/T)(dT/dr)(x^2-\frac{1}{2})$ to the square brackets of Eq. (8) and thus change the theoretical predictions for f_{peak}. We have not yet been able to determine the size of this correction due to the difficulty of obtaining accurate measurements of $T(r)$ in our low density plasma. Nevertheless, it is difficult to see how the inclusion of this term would explain the discrepancies noted at the end of Sec. III.

V. CONCLUSION

We have measured the frequency dependence of asymmetry-induced transport under very simple experimental conditions and compared the results to resonant particle theory. Our results are qualitatively consistent with the theory and support the idea that resonant particles dominate the transport, but the quantitative predictions of the simple theory employed here do not match the experiments. Apparently, the current theory does not give a complete description of this transport.

ACKNOWLEDGMENTS

This work was supported by U.S. Department of Energy Grant No. DE-FG03-98ER54457. A summer stipend for B.C. was provided by NSF-CAMP.

[1] J. S. DeGrassie and J. H. Malmberg, Phys. Fluids **23**, 63 (1980).
[2] M. H. Douglas and T. M. O'Neil, Phys. Fluids **21**, 920 (1978).
[3] J. H. Malmberg and C. F. Driscoll, Phys. Rev. Lett. **44**, 654 (1980).
[4] C. F. Driscoll and J. H. Malmberg, Phys. Rev. Lett. **50**, 167 (1983).
[5] C. F. Driscoll, K. S. Fine, and J. H. Malmberg, Phys. Fluids **29**, 2015 (1986).
[6] D. L. Eggleston, T. M. O'Neil, and J. H. Malmberg, Phys. Rev. Lett. **53**, 982 (1984).
[7] J. Notte and J. Fajans, Phys. Plasmas **1**, 1123 (1994).
[8] X.-P. Huang, F. Anderegg, E. M. Hollman, C. F. Driscoll, and T. M. O'Neil, Phys. Rev. Lett. **78**, 875 (1997).
[9] D. L. Eggleston, in *Non-Neutral Plasma Physics III*, edited by J. J. Bollinger, R. L. Spencer, and R. C. Davidson (American Institute of Physics, Melville, NY, 1999), p. 241.
[10] J. M. Kriesel and C. F. Driscoll, Phys. Rev. Lett. **85**, 2510 (2000).
[11] D. L. Eggleston and B. Carrillo, Phys. Plasmas **9**, 786 (2002).
[12] D. L. Eggleston, J. H. Malmberg, and T. M. O'Neil, Bull. Am. Phys. Soc. **30**, 1379 (1985).
[13] E. Gilson, Ph.D. thesis, University of California Berkeley, 2001.
[14] E. Gilson and J. Fajans, in *Non-Neutral Plasma Physics IV*, edited by F. Anderegg, C. F. Driscoll, and L. Schweikhard (American Institute of Physics, Melville, NY, 2002), p. 378.
[15] D. Ryutov and G. Stupakov, JETP Lett. **26**, 174 (1978).
[16] D. Ryutov and G. Stupakov, Sov. J. Plasma Phys. **4**, 278 (1978).
[17] D. Ryutov and G. Stupakov, Sov. Phys. Dokl. **23**, 412 (1978).
[18] R. Cohen, Comments Plasma Phys. Controlled Fusion **4**, 157 (1979).
[19] R. Cohen, Nucl. Fusion **19**, 1579 (1979).
[20] D. L. Eggleston and T. M. O'Neil, Phys. Plasmas **6**, 2699 (1999).
[21] J. H. Malmberg, C. F. Driscoll, B. Beck, D. L. Eggleston, J. Fajans, K. Fine, X.-P. Huang, and A. W. Hyatt, in *Non-Neutral Plasma Physics*, edited by C. W. Roberson and C. F. Driscoll (American Institute of Physics, Melville, NY, 1988), p. 28.
[22] F. Anderegg, E. M. Hollmann, and C. F. Driscoll, Phys. Rev. Lett. **81**, 4875 (1998).
[23] E. M. Hollmann, F. Anderegg, and C. F. Driscoll, Phys. Plasmas **7**, 2776 (2000).
[24] J. D. Crawford, T. M. O'Neil, and J. H. Malmberg, Phys. Rev. Lett. **54**, 697 (1985).
[25] D. L. Eggleston and J. H. Malmberg, Phys. Rev. Lett. **59**, 1675 (1987).
[26] D. L. Eggleston, Phys. Plasmas **4**, 1196 (1997).
[27] D. L. Eggleston, Phys. Plasmas **1**, 3850 (1994).
[28] J. S. DeGrassie and J. H. Malmberg, Phys. Rev. Lett. **39**, 1077 (1977).